Atmospheric Transmission Algorithm for Pulsed X-rays from High-Altitude Nuclear Detonations Based on Scattering Correction

Dinghan Zhu[1], Xiong Zhang[1], Xiaoqiang Li[1], Peng Li[1], Yanbin Wang[1] & Shuang Zhang[1*]

[1] State Key Laboratory of NBC Protection for Civilian, Beijing 102205, China

[*] 201731220010@mail.bnu.edu.cn

Author contributions

All authors contributed to the study conception and design. Material preparation, data collection and analysis were performed by Ding-Han Zhu, Xiong Zhang, Xiao-Qiang Li, Peng Li, Yan-Bin Wang and Shuang Zhang. The first draft of the manuscript was written by Ding-Han Zhu and all authors commented on previous versions of the manuscript. All authors read and approved the final manuscript.

Data Availability Statement

The data that support the findings of this study are openly available in Science Data Bank at https://cstr.cn/31253.11.sciencedb.j00186.00422 and https://www.doi.org/10.57760/sciencedb.j00186.00422 .

Abstract

In high-altitude nuclear detonations, the proportion of pulsed X-ray energy can exceed 70%, making it a specific monitoring signal for such events. These pulsed X-rays can be captured using a satellite-borne X-ray detector following atmospheric transmission. To quantitatively analyze the effects of different satellite detection altitudes, burst heights, and transmission angles on the physical processes of X-ray transport and energy fluence, we developed an atmospheric transmission algorithm for pulsed X-rays from high-altitude nuclear detonations based on scattering correction. The proposed method is an improvement over the traditional analytical method that only computes direct-transmission X-rays. The traditional analytical method exhibits a maximum relative error of 67.79% compared with the Monte Carlo method. Our improved method reduces this error to within 10% under the same conditions, even reaching 1% in certain scenarios. Moreover, its computation time is 48000 times faster than that of the Monte Carlo method. These results have important theoretical significance and engineering application value for designing satellite-borne nuclear detonation pulsed X-ray detectors, inverting nuclear detonation source terms, and assessing ionospheric effects.

Keywords: High-Altitude Nuclear Detonation; Atmospheric Transmission; Pulsed X-rays; Scattering Correction; Analytical method; Monte Carlo method

[*] Corresponding author: Shuang Zhang (E-mail: 201731220010@mail.bnu.edu.cn).

1 Introduction

Nuclear detonations can be classified into three main categories based on their location: underground or underwater, ground and surface, and low and high altitudes. High-altitude nuclear detonations differ significantly from other types of detonations [1]. According to publicly available data from the U.S. military [2], a typical low-altitude detonation mainly transmits energy through shock waves, whereas high-altitude nuclear detonations are primarily radiation driven, and the proportion of X-ray energy released (TNT equivalent) at the moment of detonation can reach up to 85% of the total equivalent [3]. Pulsed X-rays formed by high-altitude nuclear detonations serve as specific monitoring signals for such detonations [4-6]. After detonation, the X-rays interact with the atmosphere and eventually reach the satellite-borne X-ray detectors. Studying the physical processes of atmospheric X-ray transmission is essential for monitoring high-altitude nuclear detonations and detecting illegal nuclear tests under the *Comprehensive Nuclear Test Ban Treaty*.

Owing to treaty limitations, high-altitude nuclear weapon testing cannot be conducted. Therefore, current research on X-ray atmospheric transmission calculations for high-altitude nuclear detonations uses two primary methods: Monte Carlo and analytical methods. Harris et al. of the U.S. Defense Nuclear Agency developed the ATR calculation code, which uses Monte Carlo simulations to calculate the radiation environment generated by nuclear detonation X-rays and neutrons at different altitudes in the atmosphere [7]. The Ballistic Research Laboratory developed the FLAIR code, which obtains the photon energy, angle, and time for X-ray and gamma-ray transmissions using Monte Carlo database calculations [8]. Liu et al. used the Monte Carlo method to simulate the characteristic ring pinhole imaging of nuclear detonation X-rays under equivalent temperature blackbody spectra of 1.4 and 3.8 keV [9]. They established a reverse nuclear detonation equivalent table and roughly inferred the nuclear detonation equivalent through a table look-up method. Liu et al. analyzed a nuclear detonation debris cloud that generates pulsed X-rays and established a fluid dynamics model of debris motion from a near-space nuclear detonation with a TNT equivalent of 1 kt–10 Mt and a burst height of 30–80 km [10]. The results showed that the maximum height, horizontal radius, and speed of the debris cloud increase with increasing explosion height and TNT equivalent. Ou-Yang et al. used analytical numerical simulation methods to investigate the effects of nuclear detonation pulsed X-rays on the ionization and evolution of the atmosphere at different burst heights and radiation angles [11]. Xu performed analytical calculations of nuclear detonation X-ray energy deposition and demonstrated that the energy deposition is proportional to the TNT equivalent of the nuclear detonation [12]. In general, Monte Carlo methods can achieve high computational accuracy, but they are computationally expensive and cannot be applied to scenarios requiring rapid responses, such as nuclear detonation detection. Furthermore, Monte Carlo methods cannot directly infer the TNT equivalent from the output of nuclear detonation detectors. An effective way for improving both the calculation speed and inversion of the nuclear detonation equivalent is to use analytical methods. However, the current analytical methods consider only the atmospheric attenuation effect on the direct X-ray transmission orientation. Owing to their failure

to consider scattered X-rays, analytical methods have inferior calculation accuracy than Monte Carlo methods. Based on Monte Carlo simulations, Xiao et al. concluded that the high-energy nuclear detonation X-ray fluence originates mostly from non-collision X-rays, whereas the low-energy fluence originates mainly from X-rays scattered during transmission [13]. High-altitude nuclear detonations constitute a significant proportion of low-energy X-rays. Thus, it is necessary to compute scattered X-rays using analytical methods.

To address the above issue, this study established an atmospheric transmission model for pulsed X-rays in high-altitude nuclear detonations. The scattering effect was corrected using build-up factors and scattering correction coefficients. We used the proposed method to calculate the energy fluences of high-altitude nuclear detonation pulsed X-rays at different satellite altitudes, burst heights, TNT equivalents, and transmission angles.

2 Method

2.1 Nuclear detonation X-ray source

The temperature of an X-ray fireball generated by a nuclear detonation can reach 10^6–10^7 K. At this temperature, the substances in the area surrounding the detonation are completely ionized, forming high-temperature plasma [14]. The plasma exhibits a large contrast with its surroundings and can be approximated as a blackbody [3, 15]. The normalized energy spectrum can be represented by the Planck blackbody spectrum as follows:

$$P(E, T_X) = \frac{15}{(\pi \times T_X)^4} \frac{E^3}{\exp(E/T_X) - 1}, \tag{1}$$

where E is the energy of the X-ray photons and T_X is the equivalent temperature of the X-ray fireball. Assuming that $u = E/T_X$ is a dimensionless energy ratio, the normalized energy spectrum can be written as

$$P(u) = \frac{15}{\pi^4} \frac{u^3}{\exp(u) - 1}. \tag{2}$$

Some studies [16, 17] have shown that the equivalent temperature of X-ray fireballs is related to the design details of the nuclear weapon detonation processes and projectile materials. X-ray sources can be broadly divided into three categories based on the projectile type: fission bombs, ordinary hydrogen bombs, and enhanced X-ray weapons. The X-ray energy spectrum of a fission bomb can be characterized using a single blackbody spectrum with an equivalent temperature of approximately 1–2 keV. The X-ray energy spectra of other types of weapons can be characterized using composite blackbody spectra obtained by combining multiple blackbody spectra in different proportions. Here, the nuclear detonation X-ray source was a fission atomic bomb with an equivalent temperature of 1.4 keV.

2.2 Atmospheric transmission model

To calculate the parameters of nuclear detonation X-ray transmission to satellite-borne detectors, it is necessary to establish a mathematical model for nuclear detonation X-ray transmission through the atmosphere. The *U.S. Standard Atmosphere 1976* was used in the

atmospheric model in this study [18]. The atmosphere above 1000 km is extremely thin and can be considered a vacuum environment with an atmospheric density of 0. Statistically [19], the atmosphere is mostly distributed below 90 km, and the ratios of major elements (C, N, O, etc.) in the atmosphere hardly change in the 40–90 km range. The density of the atmosphere from 90 to 120 km is low, and the proportions of N and O vary, whereas the contents of the other components are very small. Monte Carlo simulations verified that the change in the proportion of each component in the atmosphere with altitude has a negligible effect (with a maximum relative error of less than 0.6% compared with the results for a fixed component) on the X-ray photon energy fluence. Therefore, it was assumed that the atmospheric composition is independent of altitude. Supposing that Earth is a standard sphere, the atmospheric density is approximated to have a spherically symmetric distribution.

The transmission parameters were calculated by establishing the transmission path relationship between detector A (where the altitude of the satellite is h_A), detonation point $B(B')$ (where the burst height is h_B), and Earth (where the spherical center is O, and the Earth's radius is R_E). δ is the observation angle, α is the transmission angle, and $AB(AB')$ is the X-ray transmission path, as shown in Fig. 1.

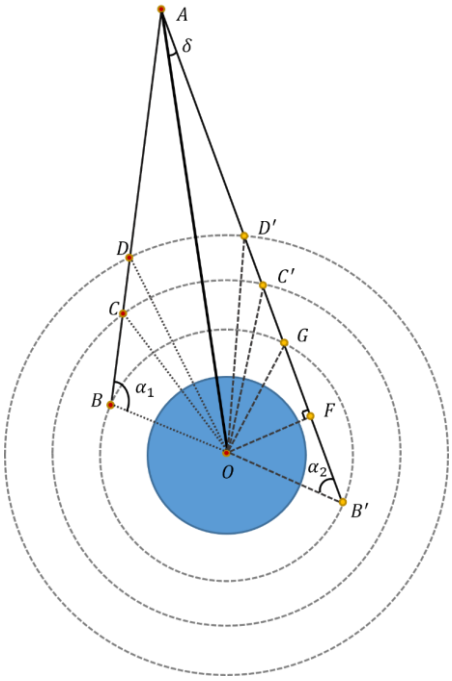

Fig. 1. High-altitude nuclear detonation X-ray transmission

2.3 Direct transmission

If a nuclear weapon detonates, X-rays interact with the atmosphere surrounding Earth layer-by-layer, starting at the detonation point, until they reach the satellite-borne X-ray detector. Nuclear detonation X-rays transmitted to satellite detectors consist of two components: directly transmitted [20] and scattered X-rays. First, we calculated the directly transmitted X-rays.

The atmosphere from the detonation point to the atmospheric boundary was assumed to be

vertically divided into $N(M)$ layers according to the 1976 standard atmosphere. The stratification height of the i-th $\left(0 \le i \le N(M)\right)$ atmosphere layer is ΔS_i. The layer containing the detonation point is the 0-th layer, with $\Delta S_0 = 0$. Other stratification heights ΔS_i are a piecewise function of altitude h:

$$\Delta S_i\left(1 \le i \le N(M)\right) = \begin{cases} 0.1, 0 \le h \le 30 \\ 2, \quad 30 < h \le 90 \\ 5, \quad 90 < h \le 1000 \end{cases}. \tag{3}$$

Calculation of the X-ray transmission attenuation requires the atmospheric column density ρ_S along the transmission path [21]. The atmospheric column density, also known as mass absorption distance, is the integral of the atmospheric density per unit length over distance. Two cases were considered for ρ_S according to the transmission angle α.

I. Case 1: Transmission angle $\alpha \ge 90°$

This case corresponds to detonation-point location B in Fig. 1. The transmission paths are $BC \to BD \to \cdots \to BA$. The layered paths are $BC \to CD \to \cdots \to A$. In this case, the transmission paths are all above the burst height h_B of point B. The total number of layers N can be written as

$$N = N_1 + N_2, \tag{4}$$

where N_1 and N_2 represent the number of layers within the 30–90 km range and 90–1000 km range, respectively.

$$N_1 = \begin{cases} \dfrac{90 - h_B}{2}, 30 \le h_B \le 90 \\ 0, \quad else \end{cases}, \tag{4a}$$

$$N_2 = \begin{cases} 182, \quad 30 \le h_B \le 90 \\ \dfrac{1000 - h_B}{5}, else \end{cases}. \tag{4b}$$

For $\triangle CBO$, according to the cosine theorem,

$$OC^2 = BC^2 + OB^2 - 2BC \times OB \times \cos\alpha, \tag{5}$$

where $OC = R_E + h_B + \Delta S_1$ and $OB = R_E + h_B$. Suppose that $BC = X_1$, and

$$X_1 = \frac{H \times \cos\alpha + \sqrt{H^2 \times \cos^2\alpha + 4\left(\Delta S_1{}^2 + H \times \Delta S_1\right)}}{2}, \tag{6}$$

where $H = 2(R_E + h_B)$, and the length ΔX_1 of the first layered path BC is

$$\Delta X_1 = X_1. \tag{7}$$

By analogy, the recurrence relation $X_n (2 \le n \le N)$ for the length of $BC \to BD \to \cdots \to BA$ is

$$X_n = \frac{H \times \cos\alpha + \sqrt{H^2 \times \cos^2\alpha + 4((\sum_{i=1}^{n} \Delta S_i)^2 + H \times \sum_{i=1}^{n} \Delta S_i)}}{2}. \tag{8}$$

The length $\Delta X_n (2 \le n \le N)$ of the n-th layered path of $BC \to CD \to \cdots \to A$ is

$$\Delta X_n = X_n - X_{n-1}. \tag{9}$$

The atmospheric column density of the transmission path in Case 1 can be expressed as

$$\rho_S(h_B, \alpha \geq 90\,^\circ) = \sum_{n=1}^{N} \Delta X_n \times \rho_V\left(h_B + \sum\nolimits_{i=0}^{n-1} \Delta S_i\right), \tag{10}$$

where $\rho_V(h)$ is the atmospheric density at altitude h.

II. Case 2: Transmission angle $\alpha < 90°$

This case corresponds to detonation-point location B' in Fig. 1. The transmission paths are $B'F \to B'G \to B'C' \to B'D' \cdots \to B'A$. The layered paths are $B'F \to FG \to GC' \to C'D' \cdots \to A$. In this case, some layered paths are partially above the burst height h_B, such as GC'; others are below h_B, such as $B'G$. To distinguish from the layers above the burst height h_B, the stratification height in section $B'G$ is expressed using Δs_i, whose physical meaning and expression are the same as ΔS_i in Equation (3).

In this case, the total number of layers M can be written as

$$M = N + M_{B'G}\,, \tag{11}$$

where N is given by Equation (4) in Case 1, and $M_{B'G}$ represents the number of layers in section $B'G$. $M_{B'G}$ is related to the shortest altitude $h_{\min}$ of the transmission path to Earth's ground and burst height h_B, where

$$OF = (R_E + h_A) \times \sin\delta = \frac{1}{2} H_A \times \sin\delta\,, \tag{12}$$

$$h_{\min} = OF - R_E. \tag{13}$$

Layer $M_{B'G}$ can be divided into three parts:

$$M_{B'G} = M_1 + M_2 + M_3, \tag{14}$$

where M_1, M_2, and M_3 represent the number of layers below 30 km, between 30 and 90 km, and between 90 and 1000 km, respectively. They can be expressed as

$$M_1 = \begin{cases} \dfrac{30 - h_{\min}}{0.1}, & h_{\min} \leq 30 \\ 0, & \text{else} \end{cases}, \tag{14a}$$

$$M_2 = \begin{cases} \dfrac{h_B - 30}{2}, & (h_{\min} \leq 30) \text{ and } (30 \leq h_B \leq 90) \\ 30, & (h_{\min} \leq 30) \text{ and } (h_B > 90) \\ \dfrac{h_B - h_{\min}}{2}, & (30 \leq h_{\min} \leq 90) \text{ and } (30 \leq h_B \leq 90) \\ \dfrac{90 - h_{\min}}{2}, & (30 \leq h_{\min} \leq 90) \text{ and } (h_B > 90) \\ 0, & \text{else} \end{cases}, \tag{14b}$$

$$M_3 = \begin{cases} \dfrac{h_B - 90}{5}, & (h_{\min} \leq 30) \text{ and } (h_B > 90) \\ \dfrac{h_{\min} - 90}{5}, & (30 \leq h_{\min} \leq 90) \text{ and } (h_B > 90) \\ \dfrac{h_B - h_{\min}}{5}, & h_{\min} > 90 \\ 0, & \text{else} \end{cases}. \tag{14c}$$

In $\triangle B'C'O$, where $B'C' = X_1$, the length ΔX_1 of the first layered path GC' above the burst

height h_B is

$$\Delta X_1 = X_1 - 2FB' = X_1 - 2\sqrt{(H/2)^2 - (H_A/2)^2 \times \sin^2\delta}\,. \tag{15}$$

The other recurrence relations for X_n and ΔX_n are the same as those in Equations (8) and (9) in Case 1.

For $B'G$ below burst height h_B, the detonation point can be equated to point F, where point B' is equivalent to the satellite. According to the geometric relationship,

$$B'G = 2B'F, \tag{16}$$

the transmission paths of section $B'F$ have a recurrence relationship similar to that of Case 1. The first-layer transmission path length x_1 and layered path length Δx_1 below the burst height h_B have the following relationship:

$$\Delta x_1 = x_1 = \sqrt{(OF + \Delta s_1)^2 - OF^2} = \sqrt{H_A \times \sin\delta \times \Delta s_1 + {\Delta s_1}^2}. \tag{17}$$

Similarly, the transmission path length x_m and layered path length $\Delta x_m (2 \le m \le M_{B'G})$ below burst height h_B have a recursive relationship:

$$x_m = \sqrt{H_A \times \sin\delta \times \sum_{i=1}^{m} \Delta s_i + \left(\sum_{i=1}^{m} \Delta s_i\right)^2}, \tag{18}$$

$$\Delta x_m = x_m - x_{m-1}. \tag{19}$$

The atmospheric column density of $B'F$ is defined as extra ρ_{S_e} and is expressed as

$$\rho_{S_e} = \sum_{m=1}^{M} \Delta x_m \times \rho_V \left(h_{\min} + \sum_{i=0}^{m-1} \Delta s_i\right). \tag{20}$$

The atmospheric column density of the transmission path in Case 2 can be written as

$$\rho_S(h_B, \alpha < 90\,^\circ) = \sum_{n=1}^{N} \Delta X_n \times \rho_V \left(h_B + \sum_{i=0}^{n-1} \Delta S_i\right) + 2\rho_{S_e}. \tag{21}$$

After calculating the atmospheric column density ρ_S for Cases 1 and 2, the X-ray transmission attenuation by the atmosphere can be calculated based on ρ_S. The mean free path of photons is a general measure of the opacity of a substance and the ability of a medium to absorb radiation [22]. The mean free path λ of X-rays with energy E between the detector and detonation point is defined as

$$\lambda(E) = \mu_m(E) \times \rho_S\,, \tag{22}$$

where $\mu_m(E)$ is the mass absorption coefficient of X-rays with energy E, which was interpolated based on discrete data provided on the official NIST website [23].

After detonation, the radiation generated by the X-ray source spreads spherically to the surrounding areas. The radiant intensity of nuclear detonation pulsed X-rays with energy E at the detector can be expressed as

$$I^{(0)}(E) = \int_{E}^{E+\Delta E} K_Q \times \frac{\eta \times Q \times f(t) \times P(E, T_X)}{4\pi \times {R_0}^2} \times e^{-\lambda(E)}\,\mathrm{d}E, \tag{23}$$

where $I^{(0)}(E)$ is the intensity of direct-transmission X-rays with energy E; K_Q is the equivalent-energy conversion factor ($K_Q \approx 2.6114 \times 10^{25}$ keV/kt), with the equivalent expressed in kt TNT; $f(t)$ is the X-ray-normalized time spectrum; R_0 is the distance from the detonation point to the satellite-borne X-ray detector; and η is the proportion of X-ray equivalent Q_X in the total detonation equivalent Q. η is related to the nuclear weapon design and its value is generally taken from 0.7 to 0.85 [3]. The expression for the relationship is as follows:

$$\eta = \frac{Q_X}{Q} . \tag{24}$$

2.4 Build-up factor

In addition to being attenuated by collisions with atmospheric particles, X-rays undergo scattering. In this study, the correction for direct-transmission orientation scattering was made using the build-up factor. Bridgman defined the build-up factor as "direct and unreacted photons plus the scattered contribution." [24] The build-up of X-ray intensity I for direct and scattered transmissions in the direct-transmission orientation comprises three components: intensity of direct transmission $I^{(0)}$, intensity after being scattered once in the direct-transmission orientation $I^{(1)}$, and intensity after $m(m \geq 2)$ scattering $I^{(m)}$.

$$I = I^{(0)} + I^{(1)} + I^{(m)}. \tag{25}$$

The single-scattering intensity was derived by Bigelow and Winfield [25], and the results of multiple scattering were derived by Renken using the Boltzmann transfer equation [26]. The relationship between the build-up factor F_B and radiation fluence in an infinite homogeneous atmosphere for X-rays with energy E is given by

$$I(E) = I^{(0)}(E) \times F_B(E). \tag{26}$$

Tayler fitted the build-up factor as a function [27] based on Monte Carlo simulation results:

$$F_B(E) = A_1 \times \exp(c_1 \times \lambda(E)) + A_2 \times \exp(c_2 \times \lambda(E)), \tag{27}$$

where A_1, A_2, c_1, and c_2 are coefficients related to the X-ray photon energy E.

The X-ray build-up factor is related to Compton scattering. Kalansky concluded that, based on the Compton scattering of photons, the value of the build-up factor can be divided into three segments depending on the X-ray energy E [28]:

I. For $E < 12$ keV, the Compton scattering is negligible, with $F_B = 1$.

II. For 12 keV $\leq$ E $\leq$ 750 keV, Talyer's fitting equation can be used and the Compton scattering cross-section of X-rays with energy greater than 100 keV starts to decrease.

III. For $E > 750$ keV, the electron pair effect is dominant, and this fitting formula is no longer applicable.

For the nuclear detonation X-ray source adopted in this study (fission atomic bomb), only approximately 1% of the X-ray energy was greater than 10 T_X, which corresponded to an energy of 14 keV. The proportion of X-rays with $E > 750$ keV was low and could be ignored [3].

The energy fluence represents the total energy of photons entering a spherical body per unit cross-sectional area during X-ray emission [29]. The initial energy fluence Φ_0 is defined as the sum of the X-ray energy fluences transmitted and scattered in the direct-transmission orientation [30]. This is the integral of the X-ray intensity over time after correction for the build-up factor.

$$\Phi_0 = \int I \, \mathrm{d}t = K_Q \times \frac{\eta \times Q}{4\pi \times {R_0}^2} \int_0^t f(t) \, \mathrm{d}t \int_0^E F_B(E) \times P(E, T_X) \times e^{-\lambda(E)} \, \mathrm{d}E \, . \tag{28}$$

When a nuclear weapon is detonated at a high altitude, the spectrum peak and duration remain in the order of nanoseconds to hundreds of nanoseconds [17]. Thus, it can be assumed that the X-ray energy spectrum does not vary with time during the observation [16]; therefore, the effect of time t was ignored.

In the direct-transmission orientation, the transmission coefficient [31] $\tau(E)$ represents the probability that an X-ray with energy E is transmitted through the atmosphere to the satellite-borne detector without considering geometric attenuation. Owing to the build-up factor, the sum of the transmission coefficients may be greater than 1. The sum of the transmission coefficients at all energies is expressed as

$$\sum \tau(E) = \sum_{E=0}^{\infty} F_B(E) \times P(E, T_X) \times \exp\left(-\lambda(E)\right) . \tag{29}$$

By ignoring the influence of time t, the initial energy fluence can be written as

$$\Phi_0 = K_Q \times \frac{\eta \times Q}{4\pi \times {R_0}^2} \times \sum \tau(E) \, . \tag{30}$$

2.5 Monte Carlo-based scattering coefficient correction

Because the nuclear detonation source can be approximated as a point source, the X-rays emitted after detonation radiate spherically toward the surrounding area. Therefore, in numerical simulations, in addition to considering the correction of direct-transmission scattering using build-up factors, it is necessary to consider the scattering effect of X-rays from other orientations. This study established a correction factor table to correct the energy fluence based on Monte Carlo simulation results. X-ray transport simulations were performed using the SuperMC Monte Carlo simulation software.

The average energy fluence $\bar{\varepsilon}$ of a single photon at the satellite altitude was calculated using Monte Carlo simulation [32]. Energy fluence Φ_{MC} can be calculated by the average energy fluence of individual photons $\bar{\varepsilon}$ amplifying the number of X-rays n_X when the detonation equivalent is Q:

$$\Phi_{MC} = n_X \times \bar{\varepsilon} \, , \tag{31}$$

where n_X can be expressed as

$$n_X = \sum_{i=1}^{W} K_Q \times \frac{\eta \times Q}{\varepsilon_i} \times \int_{E_{i-1}}^{E_i} P(E, T_X) \mathrm{d}E \, . \tag{32}$$

Here, W is the number of energy intervals, and the X-ray energy spectrum was divided into 2×10^5 energy intervals. $\varepsilon_i (1 \le i \le W)$ is the average photon energy of the i-th energy interval.

The detector counting results simulated using the Monte Carlo method were considered valid when the statistical error was within 5% [33]. The maximum permissible number of particles for each simulation condition was 2×10^9. Under these limitations, the Monte Carlo simulation results demonstrated that the lowest credible burst height was approximately 42 km.

By comparing the data of Monte Carlo simulated energy fluence Φ_{MC} with the data of initial energy fluence Φ_0, we found a strong linear relationship between the two. Therefore, X-ray energy fluence Φ at satellite altitudes can be further corrected and expressed as

$$\Phi = K(h_B) \times \Phi_0, \tag{33}$$

where K is the scattering correction coefficient related to burst height h_B (listed in Table I), and R^2 is the coefficient of determination. After testing in areas with burst heights $h_B > 100$ km, the simulation results show that $K \approx 1$ is applicable for 100 km $< h_B <$ 1500 km.

Table I. Scattering correction coefficients applicable to different heights

h_B / km	K	R^2	h_B / km	K	R^2	h_B / km	K	R^2
42	1.4550	0.9999	60	1.3168	0.9993	78	1.0625	0.9995
44	1.7756	0.9999	62	1.2717	0.9993	80	1.0513	0.9995
46	1.8236	0.9999	64	1.2329	0.9994	85	1.0454	0.9990
48	1.8479	0.9999	66	1.1985	0.9994	90	1.0477	0.9982
50	1.5682	0.9999	68	1.1675	0.9995	95	1.0214	0.9997
52	1.5362	0.9999	70	1.1401	0.9995	100	1.0071	0.9920
54	1.4864	0.9996	72	1.1160	0.9995	>100	≈1	-
56	1.4275	0.9994	74	1.0948	0.9995			
58	1.3690	0.9993	76	1.0770	0.9995			

3 Results

3.1 Comparison with Monte Carlo simulation results

The calculation conditions for the analytical simulation of the atmospheric transmission of pulsed X-rays from high-altitude nuclear detonations are listed in Table II.

Table II. Numerical simulation calculation conditions

Variable	Value and Unit	Bullet type
Satellite altitude h_A	20000 km	
Burst height h_B	42 km− 1500 km	
Transmission angle α	89°− 180°	Fission atomic bomb ($T_X = 1.4$ keV)
Detonation equivalent Q	100 kt TNT	
Proportion of the X-ray equivalent η	0.7	

For each burst height, we randomly selected no less than six transmission angles from 89, 90, 95, 100, 110, 120, 130, 140, 150, and 160° and calculated the corresponding initial energy fluence Φ_0 corrected by the build-up factor and Φ_{MC} using the Monte Carlo method. Figure 2 shows that Φ_0 and Φ_{MC} exhibit a good linear relationship. The slope of the fitting line in Fig. 2 represents the scattering correction coefficient.

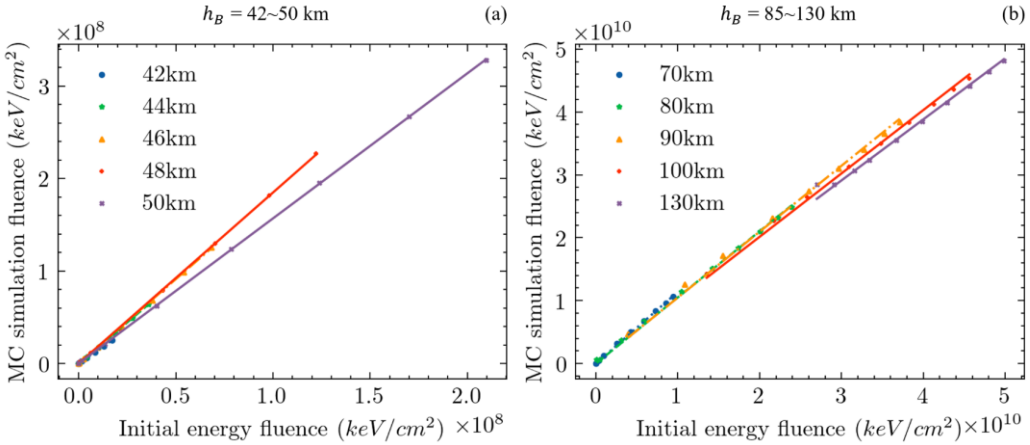

Fig. 2. Fitting diagram of initial energy fluence and Monte Carlo results

The energy fluence Φ was corrected by the build-up factor and scattering correction coefficient. For cases where the transmission angle was below 90°, the relative error between Φ and Φ_{MC} exceeded 15%, when the burst height was less than 120 km. The main reason for the large relative error in these cases is that the interaction process between the X-rays and atmosphere becomes more complex after adding the extra atmospheric column density, and the scattering process becomes more difficult to correct. If the transmission angle is appropriately selected based on different burst height conditions, the relative error is within a reasonable range (within 15% is permissible for detection), as listed in Table III.

Table III. Suggested transmission angles for different burst heights

h_B / km	Suggested availability range of α
42~64	≥ 120 °
64~74	≥ 110 °
74~90	≥ 100 °
90~100	≥ 95 °
100~130	≥ 90 °
Above 130	≥ 89 °

To validate the algorithm, we compared the proposed analytical method and another method without scattering correction with the Monte Carlo method. The results are presented in Table IV, where the uncorrected energy fluence φ is the energy fluence at the detector for direct transmission of attenuated X-rays.

Table IV. Energy fluence calculated using the Monte Carlo method, uncorrected analytical method, and proposed method

h_B / km	α /°	Energy fluence (keV/cm^2)						
		Monte Carlo energy fluence Φ_{MC}	Uncorrected energy fluence φ	Relative error between φ and Φ_{MC}	Initial energy fluence Φ_0	Relative error between Φ_0 and Φ_{MC}	Energy fluence Φ	Relative error between Φ and Φ_{MC}
42	120	2.3785×10^6	7.6610×10^5	-67.79%	1.5632×10^6	-34.28%	2.2744×10^6	-4.38%
	130	6.2691×10^6	2.3916×10^6	-61.85%	4.3270×10^6	-30.98%	6.2959×10^6	0.43%
	140	1.2065×10^7	4.9709×10^6	-58.80%	8.3617×10^6	-30.69%	1.2166×10^7	0.84%
	160	2.5130×10^7	1.1004×10^7	-56.21%	1.7199×10^7	-31.56%	2.5024×10^7	-0.42%
54	110	7.8992×10^7	3.7116×10^7	-53.01%	5.0120×10^7	-36.55%	7.4498×10^7	-5.69%
	120	2.0101×10^8	1.0322×10^8	-48.65%	1.2743×10^8	-36.60%	1.8942×10^8	-5.77%
	140	5.3173×10^8	3.1004×10^8	-41.69%	3.5159×10^8	-33.88%	5.2260×10^8	-1.72%
	150	6.9533×10^8	4.2153×10^8	-39.38%	4.6872×10^8	-32.59%	6.9670×10^8	0.20%
78	100	5.1513×10^9	4.3856×10^9	-14.86%	4.4090×10^9	-14.41%	4.6845×10^9	-9.06%

	120	1.2748×10^{10}	1.1749×10^{10}	-7.84%	1.1761×10^{10}	-7.74%	1.2496×10^{10}	-1.98%
	130	1.5688×10^{10}	1.4671×10^{10}	-6.48%	1.4682×10^{10}	-6.41%	1.5599×10^{10}	-0.57%
	140	1.8193×10^{10}	1.7172×10^{10}	-5.61%	1.7182×10^{10}	-5.56%	1.8256×10^{10}	0.35%
100	90	1.4196×10^{10}	1.3528×10^{10}	-4.71%	1.3533×10^{10}	-4.68%	1.3629×10^{10}	-4.00%
	95	2.2652×10^{10}	2.1767×10^{10}	-3.91%	2.1769×10^{10}	-3.90%	2.1924×10^{10}	-3.22%
	100	2.6434×10^{10}	2.5813×10^{10}	-2.35%	2.5814×10^{10}	-2.35%	2.5997×10^{10}	-1.65%
	110	3.1234×10^{10}	3.0919×10^{10}	-1.01%	3.0920×10^{10}	-1.01%	3.1139×10^{10}	-0.30%

Based on the data in Table IV, the results obtained by the uncorrected analytical method are significantly different from those obtained by the Monte Carlo simulation. Because the uncorrected analytical method does not consider the scattering effect, all its energy fluence values are lower than those of the Monte Carlo simulation. Under a burst height of 42 km and transmission angle of 120°, the relative error between the two reaches 67.79%. An improvement in accuracy is evident after scattering correction, with an increase of more than 60% in this case.

To further verify the accuracy, the results under different satellite altitudes, burst heights, and equivalent conditions were compared, as listed in Table V.

Table V. Verification of randomly selected different detonation equivalents and altitudes

				Energy fluence (keV/cm^2)						
Q/ktTNT	h_A/km	h_B/km	α/°	Φ_{MC}	φ	Relative error between φ and Φ_{MC}	Φ_0	Relative error between Φ_0 and Φ_{MC}	Φ	Relative error between Φ and Φ_{MC}
100	10000	60	120	2.9410×10^{9}	1.9120×10^{9}	-34.99%	2.0616×10^{9}	-29.90%	2.7147×10^{9}	-7.69%
			130	4.8608×10^{9}	3.3776×10^{9}	-30.51%	3.5544×10^{9}	-26.88%	4.6805×10^{9}	-3.71%
			150	8.8068×10^{9}	6.5290×10^{9}	-25.86%	6.7381×10^{9}	-23.49%	8.8727×10^{9}	0.75%
			160	1.0376×10^{10}	7.8116×10^{9}	-24.71%	8.0298×10^{9}	-22.61%	1.0574×10^{10}	1.91%
	10000	63	120	5.4753×10^{9}	3.8447×10^{9}	-29.78%	4.0021×10^{9}	-26.91%	5.0118×10^{9}	-8.46%
			130	8.5729×10^{9}	6.3309×10^{9}	-26.15%	6.5018×10^{9}	-24.16%	8.1422×10^{9}	-5.02%
			140	1.1731×10^{10}	8.9292×10^{9}	-23.88%	9.1088×10^{9}	-22.35%	1.1407×10^{10}	-2.76%
			150	1.4639×10^{10}	1.1358×10^{10}	-22.42%	1.1544×10^{10}	-21.15%	1.4456×10^{10}	-1.25%
	15000	45	120	2.0115×10^{7}	6.2783×10^{6}	-68.79%	1.0734×10^{7}	-46.64%	1.9317×10^{7}	-3.97%
			130	4.7660×10^{7}	1.6490×10^{7}	-65.40%	2.5733×10^{7}	-46.01%	4.6309×10^{7}	-2.84%
			150	1.2675×10^{8}	4.7031×10^{7}	-62.89%	6.7138×10^{7}	-47.03%	1.2082×10^{8}	-4.67%
			160	1.6430×10^{8}	6.1871×10^{7}	-62.34%	8.6410×10^{7}	-47.41%	1.5550×10^{8}	-5.35%
	36000	48	110	4.0104×10^{6}	1.2709×10^{6}	-68.31%	2.1608×10^{6}	-46.12%	3.9930×10^{6}	-0.43%
			120	1.2648×10^{7}	4.7400×10^{6}	-62.52%	7.0798×10^{6}	-44.02%	1.3083×10^{7}	3.44%
			140	4.1604×10^{7}	1.6980×10^{7}	-59.19%	2.2622×10^{7}	-45.63%	4.1802×10^{7}	0.48%
			160	7.0581×10^{7}	3.0006×10^{7}	-57.49%	3.8058×10^{7}	-46.08%	7.0328×10^{7}	-0.36%
200	18000	53	110	1.4151×10^{8}	6.2294×10^{7}	-55.98%	8.7038×10^{7}	-38.49%	1.3154×10^{8}	-7.05%
			120	3.7582×10^{8}	1.8078×10^{8}	-51.90%	2.3010×10^{8}	-38.77%	3.4776×10^{8}	-7.46%
			130	6.9098×10^{8}	3.5612×10^{8}	-48.46%	4.2852×10^{8}	-37.98%	6.4762×10^{8}	-6.28%
			140	1.0438×10^{9}	5.6740×10^{8}	-45.64%	6.5904×10^{8}	-36.86%	9.9600×10^{8}	-4.58%
	13000	71	110	1.5772×10^{10}	1.2566×10^{10}	-20.32%	1.2706×10^{10}	-19.44%	1.4333×10^{10}	-9.13%
			120	2.5274×10^{10}	2.1047×10^{10}	-16.72%	2.1171×10^{10}	-16.23%	2.3882×10^{10}	-5.51%
			130	3.4483×10^{10}	2.9472×10^{10}	-14.53%	2.9587×10^{10}	-14.20%	3.3376×10^{10}	-3.21%
			140	4.2982×10^{10}	3.7358×10^{10}	-13.08%	3.7467×10^{10}	-12.83%	4.2265×10^{10}	-1.67%
500	36000	83	100	1.7172×10^{10}	1.5166×10^{10}	-11.69%	1.5188×10^{10}	-11.55%	1.5914×10^{10}	-7.33%
			110	2.5966×10^{10}	2.3960×10^{10}	-7.73%	2.3974×10^{10}	-7.67%	2.5119×10^{10}	-3.27%
			120	3.2144×10^{10}	3.0240×10^{10}	-5.92%	3.0250×10^{10}	-5.89%	3.1695×10^{10}	-1.40%
			160	4.5756×10^{10}	4.4064×10^{10}	-3.70%	4.4070×10^{10}	-3.69%	4.6175×10^{10}	0.91%

The data in Table V indicate that the relative error between Φ and Φ_{MC} can be controlled within 10% by interpolating the scattering correction coefficient K for burst heights that are not listed in Table I. Moreover, the K value applies to satellite altitudes greater than 10000 km. Good agreement between the proposed analytical method and Monte Carlo simulation can be observed

for the selected available transmission angles.

The computation time [34] of the proposed analytical algorithm is reduced to 1/48000 of the time taken by the Monte Carlo method. Table VI presents a comparison of the time required by the two methods to calculate six different burst heights, with each height corresponding to 10 transmission angles in parallel.

Table VI. Comparison of calculation time between the Monte Carlo and proposed method

Calculation method	Number of simulated photons at each burst height	Calculation method	Calculation time	Calculation platform
Monte Carlo	2×10^9	Concurrent (MPI method)	3610 minutes	System: Windows7 CPU: Intel Xeon Gold 6254 (single 18 cores and 36 threads, 2pcs, total 36 cores and 72 threads) RAM: 512GB
Analytical	-	Sequential	4.5 seconds	System: Windows10 CPU: Intel Core i7-8650U (4 cores and 8 threads) RAM: 8GB

3.2 Numerical simulation calculation results

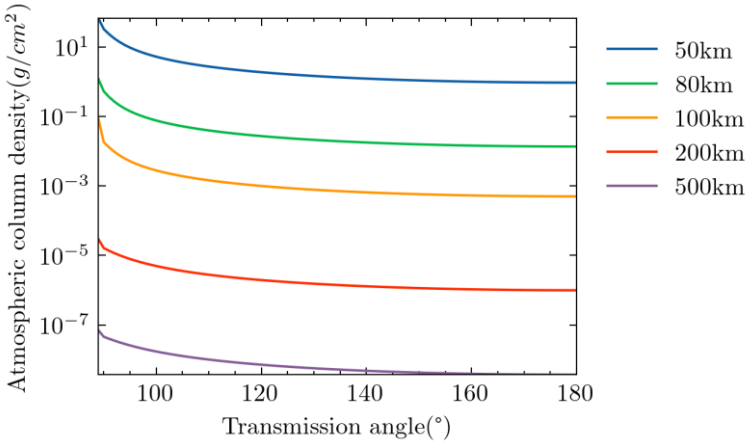

Fig. 3. Variation of atmospheric column density

First, the variation in atmospheric column density corresponding to different transmission angles for different burst heights was calculated, as depicted in Fig. 3. As the transmission angle decreases, the transmission path and atmospheric column density increase. The atmospheric column density changes considerably when the transmission angle is approximately 90°. This is because when the transmission angle is less than 90°, the X-rays pass through the low-altitude and high-density atmosphere below the detonation point, resulting in a significant increase (2 ρ_{S_e} is added) in the atmospheric column density. At different burst heights, even at the same transmission angle, the atmospheric column density differs by one order of magnitude. However, for transmission angles greater than 100°, the decrease in atmospheric column density exhibits a similar pattern of variation.

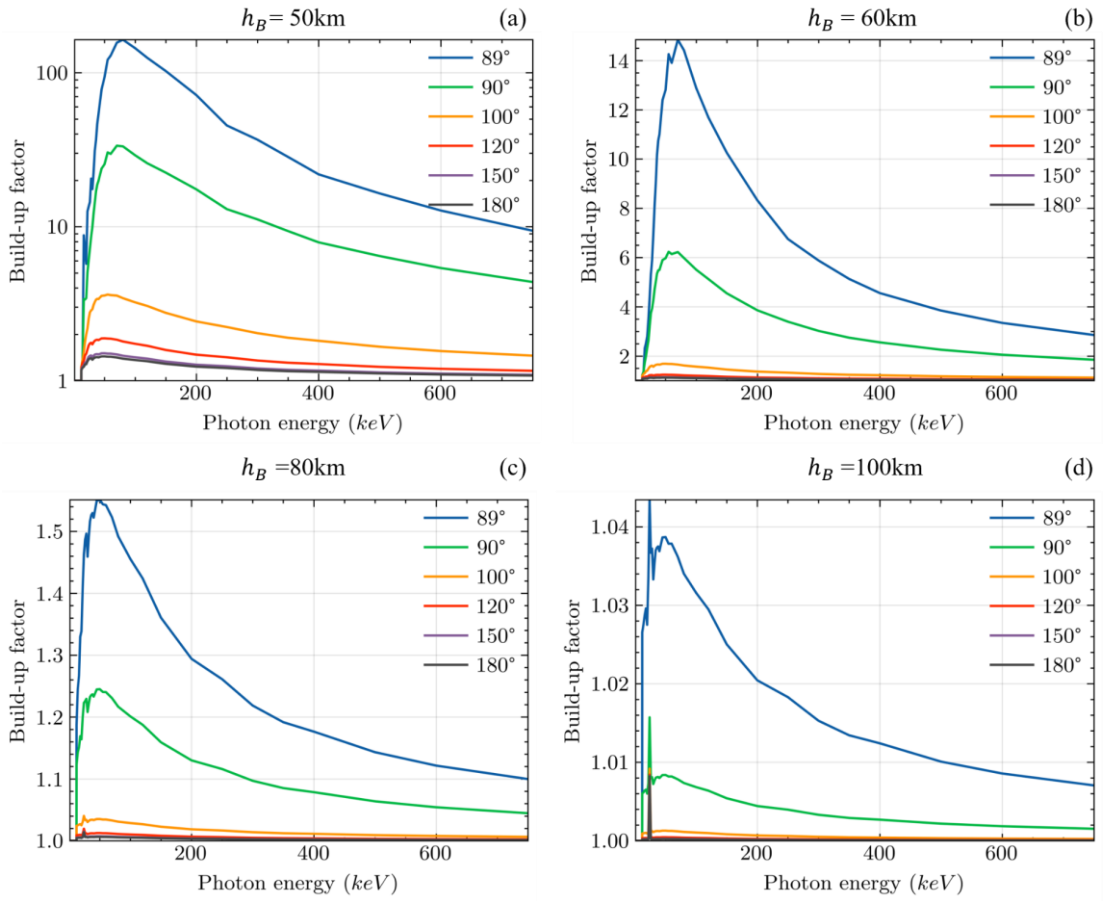

Fig. 4. Build-up factors for different burst heights and transmission angles

Subsequently, the X-ray build-up factors were calculated for different burst heights and transmission angles, as displayed in Fig. 4. The build-up factor increases from 0 to 75 keV before gradually decreasing. The burst height and transmission angle significantly affect the build-up factor. The build-up factor varies substantially for transmission angles above and below 90°. The atmospheric density is relatively high when the burst height is less than 80 km and the build-up factor is relatively large. It can be concluded that there are many scattered X-rays in the direct-transmission orientation. Moreover, X-rays in the energy band of 50–150 keV have scattering intensities exceeding direct transmission by a factor of 100 in the case of a 50 km burst height and 89° transmission angle. As the burst height increases, the atmosphere gradually becomes thinner and the scattering effect decreases. The build-up factor is close to 1 above a burst height of 100 km, and the influence of direct-transmission orientation scattering can be ignored.

Finally, as illustrated in Fig. 5, under an initial explosive equivalent $Q = 100$ kt TNT and X-ray equivalent share of 0.7, the burst height of 80 km is considered as the variation boundary. This is because the X-ray mean free path is approximately equal to the atmospheric elevation at that altitude [16]. Therefore, for detonations above 80 km, X-rays emitted upward escape from the atmosphere, whereas X-rays with burst heights below 80 km are strongly absorbed during transmission, and the entire energy emitted downward is deposited in the atmosphere. The energy fluence spans four orders of magnitude. At a burst height of 42 km and transmission angle of 120°,

the energy fluence is 2.2744 × 10^6 keV/cm^2. However, it can reach 5.9504 × 10^{10} keV/cm^2 at a burst height of 1500 km and transmission angle of 180°. These results provide a solid basis for the design of satellite-borne X-ray detectors.

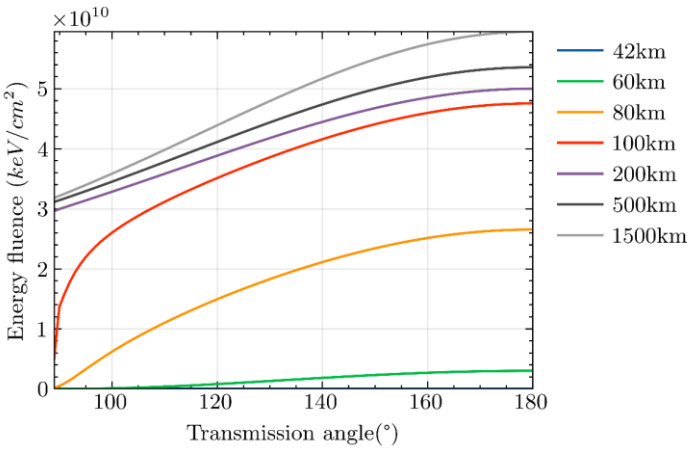

Fig. 5. Energy fluence for different burst heights and transmission angles

4 Conclusion

In this study, we developed an atmospheric transmission algorithm for pulsed X-rays from high-altitude nuclear detonations based on scattering correction. This method performs scattering correction on the energy fluence of nuclear-detonation pulsed X-rays transmitted through the atmosphere in the altitude range of 42–1500 km to a satellite at 10000–36000 km (altitude for geosynchronous satellites). We provided the recommended applicable range of the transmission angle, and the data showed good agreement between the proposed analytical method and Monte Carlo simulation for the selected available transmission angles, which can meet the requirements of high-altitude nuclear detonation monitoring. The proposed method reduced the time cost to 1/48000 of that of the Monte Carlo method. The maximum relative error between the simulation results of the traditional analytical method and Monte Carlo method was 67.79%. Using the proposed method, this error could be controlled to within 10% under the same calculation conditions, and even within 1% under certain conditions. The value of the scattering correction coefficient in the indirect-transmission orientation decreased gradually with an increase in burst height. Scattering was concentrated in the region below a burst height of 100 km, and a burst height of 80 km was considered the variation boundary of the energy fluence. The proposed method has great theoretical significance and engineering application value for the design of satellite-borne X-ray detectors, inversion of the nuclear detonation equivalent, and assessment of ionospheric effects.

References

[1] D.W Zhang, Theoretical and Laboratorial Studies of Radiative Characteristics of Soft X-rays from High-Altitude Nuclear Explosions (Changchun Institute of Optics and Precision Mechanics and Physics, Graduate School of Chinese Academy of Science, 2006). (in Chinese)

[2] Office of The Deputy Assistant Secretary of Defense for Nuclear Matters, Nuclear Matters

Handbook 2020 (2020), https://www.acq.osd.mil/ncbdp/nm//NMHB2020rev/; Accessed 20 July 2023

[3] S. Glasstone, P. J. Dolan, *The Effects of Nuclear Weapons,* 3rd edn. (US Department of Defense, 1977), pp. 27-48, 324-340. https://doi.org/10.2172/6852629

[4] X.H. Li, Y.H. Li, *Nuclear Explosion Reconnaissance Technology and Its Applications* (National Defense Industry Press, 2016), pp. 157-159 (in Chinese)

[5] X.Q. Li, Research on the Detection of Lightning Energetic Radiation and Its Influence on Nuclear Explosion Monitoring (Academy of Military Science of the People's Liberation Army, 2018) (in Chinese)

[6] R. Qiu, J.L. Li, S.Y. Zou, Developments of Nuclear Explosion Detection System on Satellite. Nucl. Electron. Detect. Tech. **25**, 887-891 (2005). https://doi.org/10.3969/j.issn.0258-0934.2005.06.082 (in Chinese)

[7] D.K. Trubey, H.E Comolander, Review of calculations of radiation transport in air: theory, techniques, and computer codes. Proceedings of a Seminar, November 15-17, 1971. (U.S. Oak Ridge National Laboratory, 1974). https://doi.org/10.2172/4668417

[8] J. Scott, B.L. Colborn, FLAIR: A Scaling and Folding Code for the Generation of Photon Transport Results in Air. Final Report (Science Applications Inc., La Jolla, USA, 1976). https://apps.dtic.mil/sti/citations/ADA034754. Accessed 20 July 2023

[9] Z.L. Liu, Y.Z. Mao, Monte Carlo Simulation on Equivalent of Nuclear Explosion Using X-ray Imaging. Chin. J. Comput. Phys. **27**, 15-22 (2010). https://doi.org/10.19596/j.cnki.1001-246x.2010.01.003 (in Chinese)

[10] L. Liu, S.L. Niu, J.H Zhu et al., Motion characteristics and laws of the debris from a near-space nuclear detonation, Nucl. Tech. **45**, 100503 (2022). https://doi.org/10.11889/j.0253-3219.2022.hjs.45.100503 (in Chinese)

[11] J.M. Ouyang, Y.Y. Ma, F.Q Shao et al., Numerical simulation of temporal and spatial distribution of X-ray ionization with high-altitude nuclear explosion, Acta Phys. Sin. **61**, 157-161 (2012). https://doi.org/10.7498/aps.61.242801 (in Chinese)

[12] H. Xu, J.M. Ouyang, S.W. Wang et al., Numerical simulation of the energy deposition of X-rays and the process of fireball radiation in the high-altitude nuclear explosion, *Paper Presented at the 2019 Annual Academic Meeting of Chinese Nuclear Society* (Baotou, Inner Mongolia, China, 2019). https://doi.org/10.26914/c.cnkihy.2019.056413 (in Chinese)

[13] Z.G. Xiao, B.Q. Tang, J.C. Gong et al., The Monte Carlo Simulation of Atmospheric Transport for γ-rays, Nucl. Electron. Detect. Tech. **3**, 283–286 (2005). https://doi.org/10.3969/j.issn.0258-0934.2005.03.015 (in Chinese)

[14] S.Y. Wang, R.Y. Zhang, L.S. Chen, Research on X-ray Radiation Field which is from a outer space nuclear explosion, Chin. J. High Pres. Phys. **3**, 50-55 (1996). http://dx.doi.org/10.11858/gywlxb.1996.03.007 (in Chinese)

[15] N. Zhou, D.J. Qiao, *Pulsed beam irradiation material dynamics* (Northwest Institute of Nuclear

Technology, 2002), pp.226-250, 281-287. (in Chinese)
[16] J.G. Wang, *Handbook of High-Altitude Nuclear Blast Effects* (Northwest Institute of Nuclear Technology, 2010). pp. 31-56. (in Chinese)
[17] D.J. Qiao, *Introduction to Nuclear Explosion Physics* (National Defense Industry Press, 1988). pp. 156-171, 258-290. (in Chinese)
[18] NASA Technical Reports Server, U.S. Standard Atmosphere 1976 (1976). https://ntrs.nasa.gov/citations/19770009539 ; 1976 [accessed 20 July 2023]
[19] G.P. Anderson, S.A. Clough, F.X. Kneizys et al., AFGL Atmospheric Constituent Profiles (0-120km) (Air Force Geophysics Laboratory, USA, 1986). https://www.researchgate.net/publication/235054307_AFGL_Atmospheric_Constituent_Profiles_0120km. Accessed 20 July 2023
[20] Y. Zheng, P. Li, N. Geng et al., *Introduction to Nuclear Explosion Monitoring Technology* (National Defense Industry Press, 2019). pp.37-43 (in Chinese)
[21] R.A. Shulstad, An Evaluation of Mass Integral Scaling as Applied to the Atmospheric Radiation Transport Problem (Air Force Inst. of Tech., Wright-Patterson AFB, OH (USA). School of Engineering, 1976), https://apps.dtic.mil/sti/citations/ADA032940. Accessed 20 July 2023
[22] C.D. Zerby, Radiation Flux Transformation as a Function of Density of an Infinite Medium with Anisotropic Point Sources (Oak Ridge National Lab., Oak Ridge, TN, USA, 1956). https://doi.org/10.2172/4337561. Accessed 20 July 2023
[23] National Institute of Standards and Technology. X-Ray Mass Attenuation Coefficients, https://dx.doi.org/10.18434/T4D01F; 2009 [accessed 20 July 2023]
[24] C.J. Bridgman, *Introduction to the Physics of Nuclear Weapons Effects* (Fort Belvoir, VA: Defense Threat Reduction Agency, USA, 2001). p.209
[25] J.R. Bigelow, S. Winfield Photon Transport from a Point Source in the Atmosphere (Air Force Inst. of Tech., Wright-Patterson AFB, OH (USA). School of Engineering, 1968). https://apps.dtic.mil/sti/citations/AD0838387. Accessed 20 July 2023
[26] J.H. Renken, *Transmission of X-rays Through AIR* (Sandia Corp., Albuquerque, N. Mex., 1965). pp.7-46
[27] J.J. Taylor, *Application of Gamma Ray Build-Up Data to Shield Design* (Westinghouse Electric Corp. Atomic Power Div., Pittsburgh, 1954).
[28] G.M. Kalansky, X-ray Build-Up Factors, (Air Force Inst. of Tech., Wright-Patterson AFB, OH (USA). School of Engineering, 1978)
[29] J.F. Qian, T.Y. Shen, *Nuclear radiation dosimetry* (National Defense Industry Press, 2009), p.3
[30] A.E. Green, T.R. Peery, R.C. Slaughter et al., Physical Modeling of Nuclear Detonations in DIRSIG, *Paper Presented at the 2014 IEEE Applied Imagery Pattern Recognition Workshop (AIPR)* (IEEE, Washington, DC, USA, 2014), pp. 1-6. https://doi.org/10.1109/AIPR.2014.7041907
[31] D.E. Jones, X-Ray Fluence and Transmission and Prompt Radiation Fluence or Dose. Master's Thesis (Air Force Inst. of Tech., Wright-Patterson AFB, OH (USA). School of Engineering, 1981)

[32] Y.H. Zhang, Nonrecursive residual Monte Carlo method for SN transport discretization error estimation. Nucl. Sci. Tech. **33**, 61(2022). https://doi.org/10.1007/s41365-022-01042-w.

[33] J.A. Kulesza, T.R. Adams, J. C. Armstrong et al., MCNP Code Version 6.3.0 Theory & User Manual (Los Alamos National Laboratory Tech. Rep. LA-UR-22-30006, Rev. 1. Los Alamos, NM, USA, 2022). https://doi.org/10.2172/1889957

[34] S.C. Zheng, Q.Q. Pan, H.W. Lv et al., Semi-empirical and semi-quantitative lightweight shielding design algorithm. Nucl. Sci. Tech. **34**, 43 (2023). https://doi.org/10.1007/s41365-023-01187-2.